

Phase stability and bonding characteristics of Li-rich Al-Li intermetallic compounds: Al_2Li_3 and Al_4Li_9

X.-Q. Guo, R. Podloucky,* and A. J. Freeman

Department of Physics and Astronomy, Northwestern University, Evanston, Illinois 60208-3112

(Received 12 June 1990)

The all-electron local-density full-potential linearized augmented-plane-wave method was applied to calculate the total energy and electronic structure of several Li-rich Al-Li compounds including Al_2Li_3 , Al_4Li_9 , and AlLi_3 (with $L1_2$ and $\text{D}0_3$ structure). The ground-state properties are found to be in good agreement with the available experimental data. Based on the calculated heats of formation, both Al_2Li_3 and Al_4Li_9 were found to be stable, whereas both AlLi_3 compounds are unstable with respect to the mixture of the most stable compounds. The bonding in the stable phases is characterized by its tendency to form stronger, tetrahedra-like Al—Al bonds due to the Al-Al and Al-Li interactions. Based on these results, we propose that the phase stability and the bonding characteristics of the Al-Li alloys can be understood by assuming that the Li atoms basically transfer their valence electrons in between the Al bonds and that the resultant strengthened Al bonds stabilize the Al-Li compounds.

I. INTRODUCTION

Although the Li-rich side (i.e., greater than 50 at. % Li) of Al-Li alloys is less important for practical applications than the Al-rich side (which are the promising high-strength, low-density materials for the aerospace industry¹⁻⁴), first-principles band calculations of some of the Li-rich Al-Li ordered compounds are important for the following reasons. First, the calculation of alloy phase diagrams with a combination of first-principles electronic-structure calculation and thermodynamic statistics has become a realistic and exciting possibility due to the development of precise energy-band calculation methods and the rapid increase of computer power. For example, calculations of the Al-Li phase diagram have been done from first principles by combining highly precise results of full-potential linearized augmented-plane-wave (FLAPW) electronic total-energy calculations of the Al-Li compounds with a statistical supercell method⁵ and (more impressively) with the cluster variation method.⁶ The calculations correctly produced and predicted many structural, cohesive, and thermodynamic properties on the Al-rich side of the Al-Li alloys and the agreement with experiment is encouraging. However, the results for the Li-rich side are less satisfactory. Since these calculations involved only fcc or bcc superstructures which are not the actual stable phases on the Li-rich side, they could not produce the correct phase diagram on the Li-rich side. Some of the more complicated noncubic structures such as Al_2Li_3 and Al_4Li_9 , which are found experimentally to be stable phases, were not included. Therefore, for the completion of the Al-Li phase diagram, the calculation of these noncubic structures to the same level of precision is desirable.

Second, although both Al and Li are simple metals and are usually considered to be more or less free-electron-like, the structures and the bonding characteristics of

their intermetallic compounds differ significantly from their parent compounds. For example, AlLi crystallizes in the rather rare $B32$ ($Zn\text{t}1$) phase instead of the more common $B2$ (CsCl) phase due to strong local-environment and chemical-bonding effects; this was found by both experiment and theoretical calculations.⁷⁻¹⁰ When the Li content is increased, the structure of Al-Li alloys changes from pure fcc Al, to an fcc Al-Li solid solution and an fcc-based Al_3Li ($L1_2$ metastable) phase to a bcc-based AlLi ($B32$) structure. On the Li-rich side, the situation is more complicated. The structure changes from the bcc-based $B32$ structure to rhombohedral Al_2Li_3 ($C33$) and to monoclinic Al_4Li_9 ($B2/m$).

This trend of the change of structures among Al-Li intermetallic compounds indicates that the unusual nature of Li might have great impact on the bonding characteristics of Al-Li compounds, especially when the Li content is increased. So far, there is no theoretical study of the Li-rich Al-Li compounds and the number of experimental studies is also limited; reliable information, such as bulk modulus and cohesive energy, is lacking. Therefore, to complete the study of the phase stabilities and bonding properties of Al-Li alloys, first-principles total-energy calculations on some of the Li-rich Al-Li intermetallic compounds are necessary. Thus this study is part of the extensive investigation on the Al-Li alloys and the results might serve as reference for the phase stability on the Li-rich side of the alloys. Finally, the unusual bonding characteristics of Al-Li compounds is strongly pronounced by the Al-rich compounds.

II. COMPUTATIONAL DETAILS

The first-principles self-consistent all-electron full-potential linearized augmented-plane-wave method,¹¹ within the local-density approximation^{12,13} (LDA) with

use of the exchange-correlation potential of Hedin and Lundqvist,¹⁴ was applied to calculate the electronic structures and volume-dependent total energies of Al_2Li_3 and Al_4Li_9 . Two artificial AlLi_3 compounds with fcc-based $L1_2$ and bcc-based DO_3 structure and an fcc-based eight-atom supercell structure (denoted as a 2:6 compound), usually used for the phase diagram calculation,^{5,6} are considered for comparison. Muffin-tin radii were chosen as 2.44 a.u. for Al_2Li_3 and Al_4Li_9 and 2.58 a.u. for the artificial AlLi_3 compounds. The charge density and potential were expanded in spherical harmonics inside muffin-tin spheres up to $l=6$ for Al_2Li_3 and Al_4Li_9 and $l=8$ for the AlLi_3 compounds. The number of plane waves for the representation of charge density and potential in the interstitial region is about 4000, 8000, and 2000 for Al_2Li_3 , Al_4Li_9 and AlLi_3 , respectively, which is proportional to the corresponding volume of the interstitial region. The number of basis functions used to build up the Hamiltonian is about 50 per atom in each case. Since in the FLAPW method all the parameters are fully controlled, the choice of the parameters will not affect the results provided that they are sufficiently well converged.

To test the results at certain volumes, we increased the number of basis functions (to 100 per atom), and also other parameters, and the total-energy difference was found to be less than 0.1 mRy. The number of \mathbf{k} points in the irreducible Brillouin-zone used by the linear tetrahedron method for Brillouin-zone integration is about 60, which yields sufficient precision for calculations of the equilibrium lattice constants and bulk moduli. The absolute total energies at equilibrium were obtained by a systematic increase of the number of \mathbf{k} points and an extrapolation method.¹¹

III. RESULTS

A. Crystal structures and lattice constants

The crystal structures of Al_2Li_3 , Al_4Li_9 , and two artificial AlLi_3 compounds are shown in Fig. 1. Al_2Li_3 crystallizes in the rhombohedral structure ($C33$) [as shown in Fig. 1(a)] with space group $R\bar{3}m$. There is one formula unit in the rhombohedral unit cell or three formula units in a hexagonal unit cell. The experimental lattice constants in the rhombohedral cell are¹⁵ $a=10.2406$ a.u. and $\alpha=49.16^\circ$, which corresponds to a c/a ratio of 3.163. The atomic positions in the unit cell are listed in Table I. In the calculation, the experimental values of α (and therefore the c/a ratio) and the relative atomic positions are chosen and fixed, which is a reasonable compromise to get accurate results and, at the same time, to avoid too many calculations due to the variation of c/a and atomic positions. Although the traditional overestimate of bonding by LDA produces smaller lattice constants than experiment, the error is considered systematic and therefore has little effect on the c/a ratio and relative atomic positions inside the unit cell. We tested the results by changing the value of α and found that the equilibrium α is indeed sufficiently close to experiment. Similar tests were done on other aluminide compounds by Hong¹⁶ for varying c/a and by Xu¹⁷ for varying atom-

TABLE I. Atomic positions for Al_2Li_3 in Cartesian coordinates.

Atom type	x	y	z
Al	0	0	0.1964
	0	0	-0.1964
Li(1)	0	0	0
Li(2)	0	0	0.4015
	0	0	-0.4015

ic positions and the results showed that the choice of the experimental values of the c/a ratio and the atomic positions is in general reasonable in first-principles calculations.

The crystal structure of Al_4Li_9 is monoclinic with space group $B2/m$, as shown in Fig. 1(b). There are two formula units in a simple monoclinic unit cell but only one formula unit in the base-centered monoclinic unit cell. The experimental lattice constants¹⁸ are $a=36.198$ a.u., $b=10.259$ a.u., $c=8.502$ a.u., and $\gamma=107.671^\circ$. Again, the experimental values of γ and atomic positions are used in the calculation, as in the case of Al_2Li_3 . There are two types of Al and five types of Li due to the different local environments and the atomic positions in the unit cell are listed in Table II.

The crystallographic structures of the artificial AlLi_3 compounds are more common: $L1_2$ -structure AlLi_3 [Fig. 1(c)] has an fcc superstructure with space group $Pm\bar{3}m$; there are four atoms in a unit cell with Al sitting at the corners and Li sitting on the face centers. The 1:3 compound of DO_3 -structure AlLi_3 structure [Fig. 1(d)] has a bcc superstructure with space group $Fm\bar{3}m$; there are also four atoms in a unit cell which can be considered as

TABLE II. Atomic positions for Al_4Li_9 in Cartesian coordinates.

Atom type	x	y	z
Al(1)	0.1505	0.0870	0
	-0.1505	0.087	0
Al(2)	0.3853	0.7064	0
	-0.3853	-0.7064	0
Li(1)	0	0	0
Li(2)	0.0863	0.5310	0
	-0.0863	-0.5310	0
Li(3)	0.2326	0.6220	0
	-0.2326	-0.6220	0
Li(4)	0.3080	0.1440	0
	-0.3080	-0.1440	0
Li(5)	0.4565	0.2390	0
	-0.4563	-0.2390	0

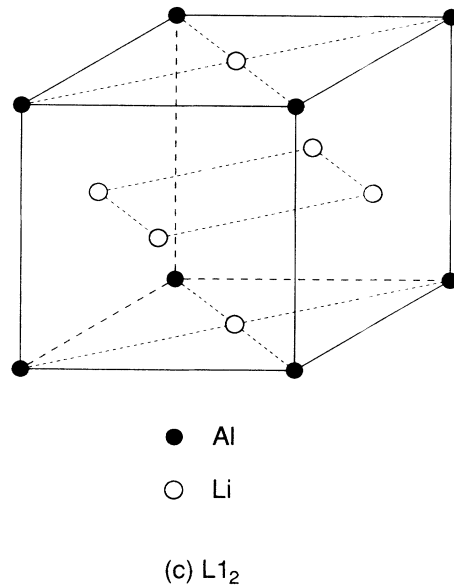
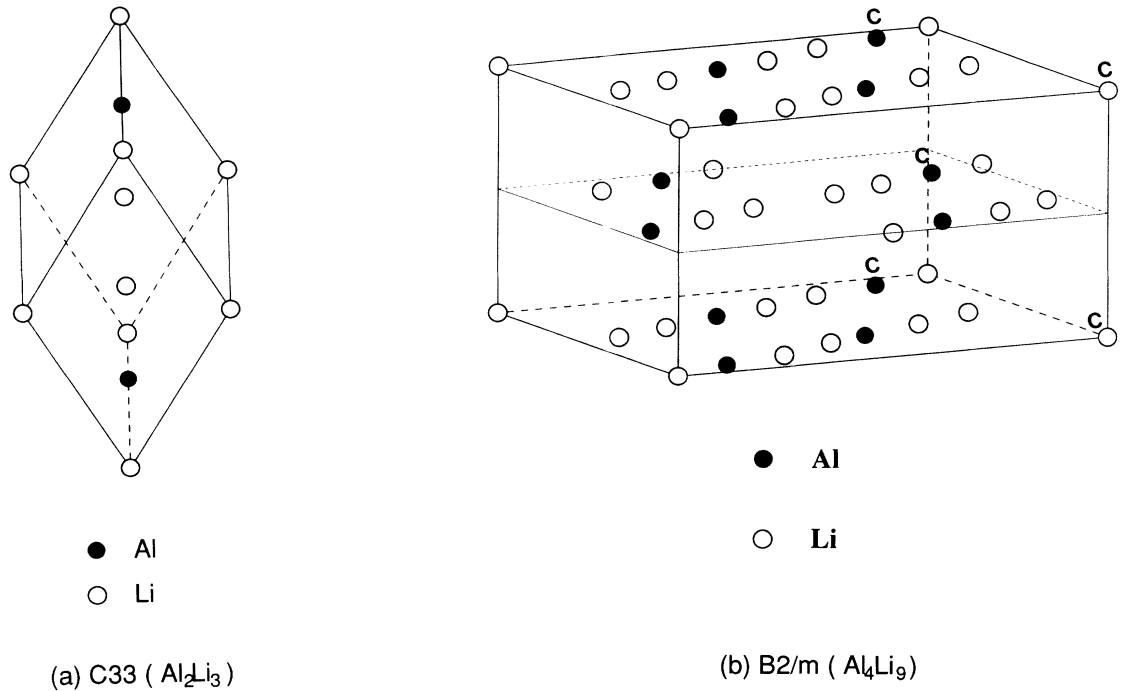


FIG. 1. Crystal structures of (a) Al_2Li_3 (with C33 structure), (b) Al_4Li_9 (with monoclinic structure), (c) AlLi_3 ($L1_2$), (d) AlLi_3 ($D0_3$), and (e) Al_2Li_6 fcc supercell. In (a) the orientation shown emphasizes that the z axis is defined by the line connecting the Al atoms, the innermost Li atoms, and the two Li atoms at the top and bottom of the figure. It does not coincide with any edges of the rhombohedron. In (b) the atomic arrangement of the central plane is the same as for the basal plane but shifted by $\frac{1}{2}$ of the a axis. The atoms labeled c lie in the plane of the contour plot of Fig. 3(b) shown later.

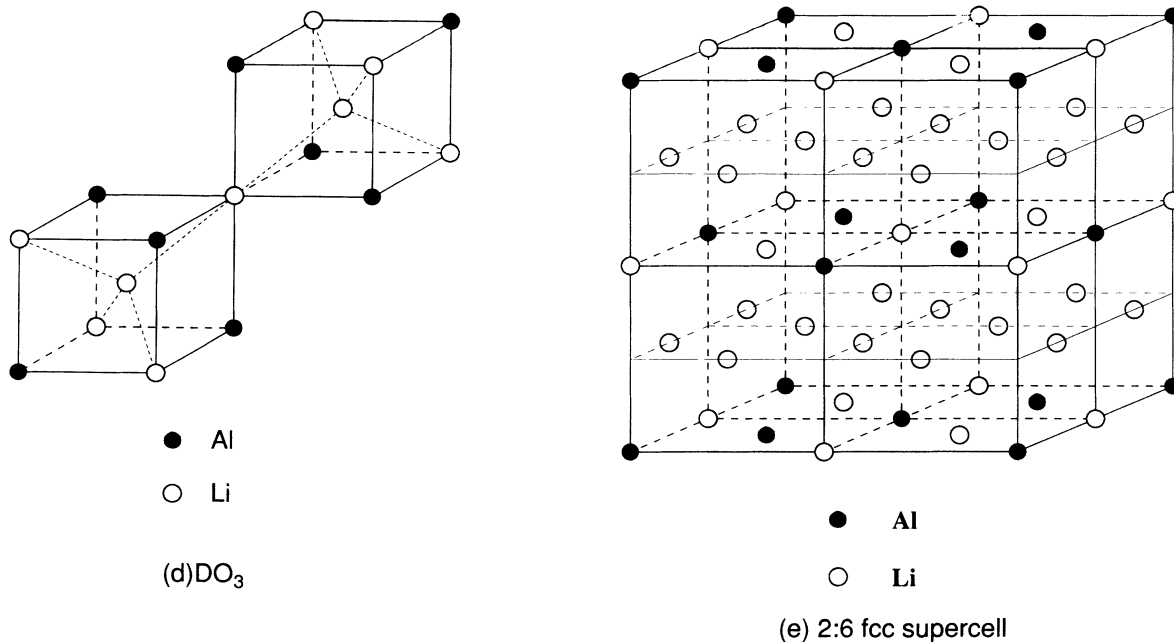


FIG. 1. (Continued).

one Al and three Li fcc sublattices interpenetrating along the [111] direction. The structure of the fcc-based 2:6 compound, which can be realized only by the supercell approach,⁵ is shown in Fig. 1(e).

B. Equilibrium ground-state properties

The calculated equilibrium lattice constants of Al₂Li₃ and Al₄Li₉ are given in Table III, along with experimental data and relative errors. Results for pure Al and Li are also included. The lattice constants for pure Al and Al₂Li₃ are in good agreement with experiment (within

2%). The 2.7% relative error for Al₄Li₉ is considerably larger, whereas pure Li has the largest relative error (about 4%). It should be noted that (i) the calculated lattice constants are systematically smaller than experiment and (ii) the error is increased when the Li content is increased. The discrepancy between the theoretical and experimental results may be attributed to several reasons. First, it might be due to the effect of thermal expansion, since the calculated results are valid at $T=0$ K. To investigate the effect of thermal expansion due to the anharmonic behavior of lattice vibrations, we used the experimental thermal expansion coefficients¹⁹ for pure Al

TABLE III. Comparison of calculated lattice constants a_{calc} in a.u. with experimental values a_{expt} for Al-Li ordered compounds.

Composition	Structure	a_{calc}	a_{expt}	Rel. error
Al	fcc	7.538	7.636 ^c	1.28%
Al ₂ Li ₃	C33	8.397 (a)	8.518 (a) ^a	1.42%
		26.561 (c)	26.946 (c)	
Al ₄ Li ₉	B2/m	35.221 (a)	36.198 (a) ^b	2.7%
		9.982 (b)	10.259 (b)	
		8.272 (c)	8.502 (c)	
		107.67 (γ)	107.67 (γ)	
Li	bcc	6.35	6.631 ^c	4.22%
			6.614 (77 K) ^c	3.99%
Li	fcc	8.00	8.334 (77 K) ^c	4.01%

^aExperimental data taken from Ref. 15.

^bExperimental data taken from Ref. 18.

^cExperimental data taken from Ref. 19.

TABLE IV. Temperature dependence of experimental coefficients of linear thermal expansion α of pure Al and Li (in units of 10^{-6} K^{-1}).

Material	25 K	50 K	75 K	100 K	150 K	200 K	250 K	300 K
Al	0.5	3.8	8.2	12.2	17.2	20.2	21.9	23.2
Li			13.0	21.2	32.5	39.3	43.8	47.0

and Li (as listed in Table IV) and extrapolated the calculated results from zero to room temperature. We found that this effect contributes to about $\frac{1}{3}$ of the error for pure Al and $\frac{1}{4}$ of the error for pure Li. (In other words, the calculated lattice constant will increase about 0.5% for pure Al and 1% for pure Li if this effect is taken into account.) Second, the neglect of the zero-point energy might cause considerable error in the calculated lattice constants in some cases. The zero-point energy is greater when the volume is smaller and therefore acts like an effective repulsive force. The calculated equilibrium lattice constants will be increased if this term is included. Recently, Moruzzi *et al.*²⁰ applied the less precise augmented-spherical-wave (ASW) band-structure approach and obtained larger lattice constants for several elements when the zero-point energy was included by a semiempirical Debye model. The effect of the zero-point-energy contribution is more important for lighter elements, which appears to be the reason that the theoretical lattice constant of Li has the largest error in comparison with experimental data. Third, there are other approximations that might also affect the results; traditionally, it is assumed that the LDA overestimates the bonding in most cases.

The Wigner-Seitz radii, bulk moduli, and cohesive energies are listed in Table V. The Wigner-Seitz radii (corresponding to the equilibrium volume per atom) of Li-rich ordered compounds (up to 75 at.% Li concentration) are only slightly larger than that of pure Al (with a difference of less than 1%), even though pure Li has a much larger Wigner-Seitz radius than does pure Al (about 6%). The strong deviation from Vegard's law is well known for Al-Li alloys and highlights the unusual bonding properties of these alloys. The bulk moduli, on the other hand, decrease almost linearly as the Li concentration increases. They are very close to the linear inter-

polation of the bulk modulus of pure Al and Li, i.e., $B(x) = xB_{\text{Al}} + (1-x)B_{\text{Li}}$, as found for the Al-rich side of the Al-Li solid solution⁵ and ordered compounds.^{10,21}

C. Density of states

The densities of states (DOS) for the AlLi_3 ($D0_3$), AlLi_3 ($L1_2$), Al_2Li_3 , and Al_4Li_9 compounds are shown in Fig. 2. The DOS and the integrated DOS at the Fermi energy are listed in Table VI.

The densities of states of $D0_3$ and $L1_2$ [Figs. 2(a) and 2(b)] have some similarities. The Al s and p states are almost completely separated, and are totally different from the free-electron-like compounds such as Al_3Li . The Al s states are well localized at the lowest energy while the Al p states occupy the higher energy around E_F . In both cases, the Al-Al interaction is very weak because there are no Al-Al nearest neighbors and Al atoms look more like impurities in both structures. The Al-Li and Li-Li interactions are mainly responsible for the cohesion of these structures. In the $D0_3$ case, the interaction is stronger and a gap is opened up separating the bonding and antibonding states. The Fermi energy is lower in the $D0_3$ case. The valence electron energy and the kinetic energy are lower in the $D0_3$ structure, which lowers its total energy and therefore makes the $D0_3$ structure more stable than the $L1_2$ structure.

The density of states of Al_4Li_9 [Fig. 2(c)] is quite different from those of the AlLi_3 compound, but is instead more similar to that of the $B32$ -structure AlLi compound, although its Li composition is much closer to AlLi_3 . There are three main peaks below E_F as in the case of $B32$ -structure AlLi . The first peak, dominated by Al s states, arises from the Al-Al s bonding state with some hybridization with Li. The second peak is also mainly Al s , but with a sizeable mixture of Al p and Li s

TABLE V. Calculated equilibrium Wigner-Seitz radii R_{WS} (in a.u.), total energies E_{tot} (in Ry/atom), bulk moduli B (in Mbar), cohesive energies ΔH_{coh} (in Ry/atom), and heats of formation ΔH_{form} (in mRy/atom) of some Li-rich ordered compounds and pure Al and Li.

Composition	Structure	R_{WS}	E_{tot}	B	ΔH_{coh}	ΔH_{form}
Al_2Li_3	$C33$	2.9592	-202.4521	0.44	-0.2074	-14.2
Al_4Li_9	$B2/m$	2.9420	-159.1560	0.34	-0.1885	-11.2
AlLi_3	$D0_3$	2.9588	-132.0948	0.30	-0.1754	-7.9
	$L1_2$	2.9647	-132.0915	0.28	-0.1721	-4.6
Al	fcc	2.9460	-483.8420	0.82	-0.2950	
Li	fcc	3.1246	-14.8352	0.14	-0.1250	
	bcc	3.1276	-14.8347	0.15	-0.1245	

and p states. The third broad peak just below E_F is the strong hybridization between Al p and Li p states. The distinctive difference between $B32$ -structure AlLi and Al_4Li_9 is the DOS just above E_F . In $B32$ -structure AlLi, the Fermi energy just falls in the deep valley between two big peaks, while in Al_4Li_9 , there is a broad valley (0.12 Ry) between two big peaks, which separates the bonding and antibonding states. The more complicated shape of the density of states of Al_4Li_9 is due to its more complex

structure. A more detailed discussion on the relation between the structure of $B32$ -structure AlLi and Al_4Li_9 will be given later.

The density of states of Al_2Li_3 [Fig. 2(d)] is again similar to that of $B32$ -structure AlLi with three distinctive peaks below E_F . The composition of Al_2Li_3 (60 at. % Li) is closer to the 50 at. % Li for $B32$ -structure AlLi and hence a similarity should be expected. There is a gap opening up between the lowest two peaks which separates

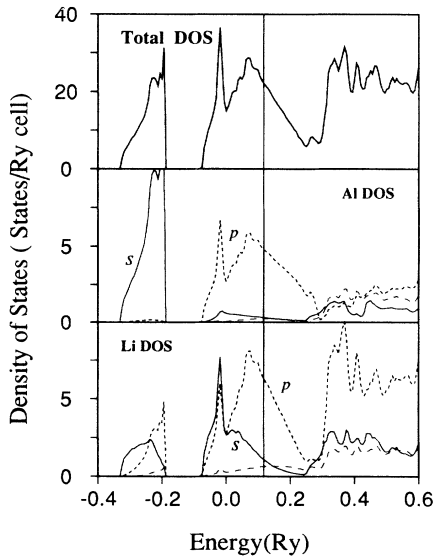
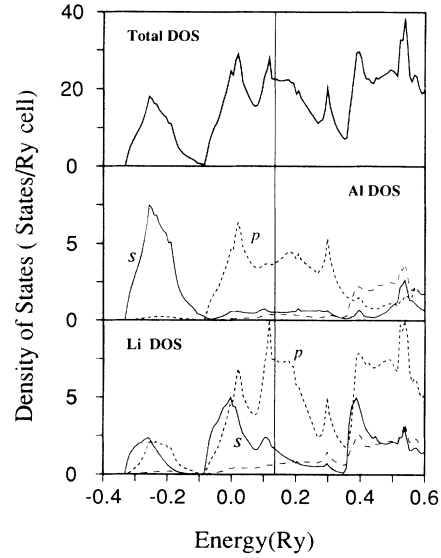
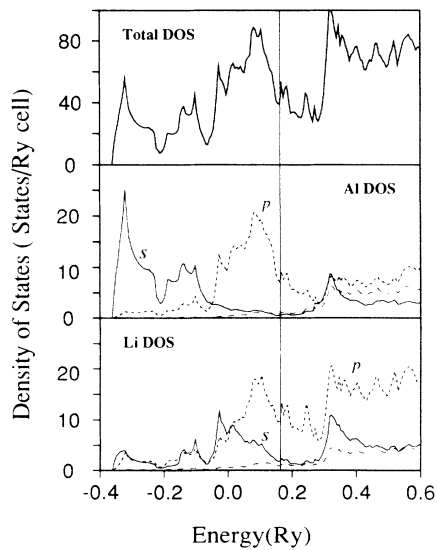
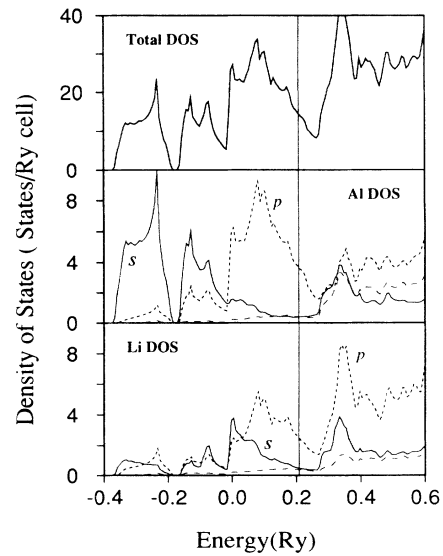
(a) $AlLi_3$ - DO_3 (b) $AlLi_3$ - $L1_2$ (c) Al_4Li_9 (d) Al_2Li_3

FIG. 2. Total density of states and l decomposition of density of states for (a) the $AlLi_3$ (DO_3) structure; (b) the $AlLi_3$ ($L1_2$) structure, (c) the Al_4Li_9 compound, and (d) the Al_2Li_3 compound.

TABLE VI. Density of states for the four Li-rich compounds decomposed into contributions from the interstitial region (int) and from the spheres. The first (top) block [$N(E_F)$] corresponds to the density of states at the Fermi energy, and second (bottom) block (n) lists the integrated values.

Structure	Total		Al				Li			
	N	N_{int}	N_s	N_p	N_d	N_{sph}	N_s	N_p	N_d	N_{sph}
$L1_2$	22.58	8.06	0.54	3.74	0.37	4.67	1.68	7.43	0.65	9.77
DO_3	22.22	8.76	0.31	4.80	0.23	5.35	1.08	5.31	0.64	7.04
Al_4Li_9	39.12	18.13	0.47	6.72	0.79	7.89	1.81	9.86	0.91	12.6
Al_2Li_3	14.35	6.56	0.38	3.62	0.40	4.42	0.77	2.48	0.39	3.65
	n	n_{int}	n_s	n_p	n_d	n_{sph}	n_s	n_p	n_d	n_{sph}
$L1_2$	6.00	2.10	0.94	0.78	0.03	1.75	0.84	1.18	0.1	2.03
DO_3	6.00	2.30	0.89	0.79	0.02	1.70	0.76	1.12	0.09	1.97
Al_4Li_9	21.0	9.12	3.14	3.35	0.17	6.66	1.94	2.98	0.25	4.19
Al_2Li_3	9.0	3.97	1.54	1.65	0.10	3.30	0.51	1.01	0.10	1.63

the s and p bonding and antibonding states, while in the $B32$ -structure $AlLi$ case, such a gap is prohibited due to the diamond symmetry.

There are some common features at E_F for the Li-rich compounds which distinguishes them from the $B32$ -structure $AlLi$ compounds. First, the s and d DOS components at E_F are greatly depressed for the Li-rich compounds and the DOS at E_F is predominately composed of Al and Li p states (about 70–80%), whereas in the $B32$ case, p only occupies $\frac{1}{3}$ of the states. In the Li-rich compounds, s electrons mainly occupy the lower bands while p electrons occupy the higher bands around E_F , which are well separated. Second, the structure induced d component of the electron states is less pronounced in the Li-rich compounds than in the $B32$ -structure $AlLi$ compounds. The percentage of d electrons is decreased as the Li concentration increases, which is expected because Li is less likely to induce d components than Al.

D. Charge density and bonding characteristics

Although Al_2Li_3 and Al_4Li_9 have complex crystal structures, their similarity with the bcc structure is apparent if we carefully study their structures. The structure of Al_2Li_3 can be looked at as a variant of bcc packing with Al atom layers of puckered six membered rings, with the [111] direction of the bcc cube taken as the z direction, as shown in Fig. 1(a). The calculated nearest atomic distances are listed in Table VII. For each atom in the unit cell, if we consider these neighboring atoms with distance of about 5.2 a.u. as its nearest neighbors and distances of about 6.0 a.u. as its next nearest neighbors, then there will be eight nearest neighbors and six next nearest neighbors for each atom. The ratio of average nearest-neighbor distance (5.198 a.u.) to the next-nearest-neighbor distance (6.014 a.u.) is 0.864, which is very close to the ideal ratio of 0.866 for the bcc structure. Each Al atom has three Al nearest neighbors similar to the tetrahedral bonding in $B32$ -structure $AlLi$, but with one Al—Al bond missing. The striking feature in this compound is that its Al-Al neighbors have the smallest distances (5.101 a.u.) in the compound, which is smaller than those in pure Al (5.33 a.u.) and even slightly smaller

than those in $B32$ -structure $AlLi$ (5.119 a.u.). Figure 3(a) shows charge density contours for Al_2Li_3 on the y - z plane, which contains Al-Al nearest neighbors. We see a strong pileup of the charge density in the area between the Al atoms. Al—Al bonding is strengthened by the charge transfer of Li into the bonding region and this is as strong as in the case of $B32$ -structure $AlLi$. The similarity of strengthened Al—Al bonds in both Al_2Li_3 and $B32$ -structure $AlLi$ might be the reason for Al_2Li_3 's stability on the Li-rich side of the Al-Li phase diagram.

Al_4Li_9 is more complicated with a monoclinic structure and more atoms in the unit cell. Basically, however, it can also be looked upon as a distorted bcc superstructure with a more complicated local orientation. The calculated nearest neighbors and next nearest neighbors are listed in Table VIII. There are fourteen neighbors with shortest but different distances which can be grouped into eight nearest and six next nearest neighbors as in the case of Al_2Li_3 . Again the ratio of the average nearest and next

TABLE VII. Atomic distances (in a.u.) and the coordination number (CN) in Al_2Li_3 .

Atom	Neighbor	Distance	CN
Li(1)	Li(2)	5.175	6
	Al	5.218	2
	Al	6.060	6
Li(2)	Li(1)	5.175	3
	Li(2)	5.233	1
	Al	5.181	3
	Al	5.447	1
	Li(2)	6.053	3
	Al	5.926	3
Al	Li(1)	5.218	1
	Li(2)	5.181	3
	Li(2)	5.447	1
	Al	5.101	3
	Li(1)	6.060	3
	Li(2)	5.926	3

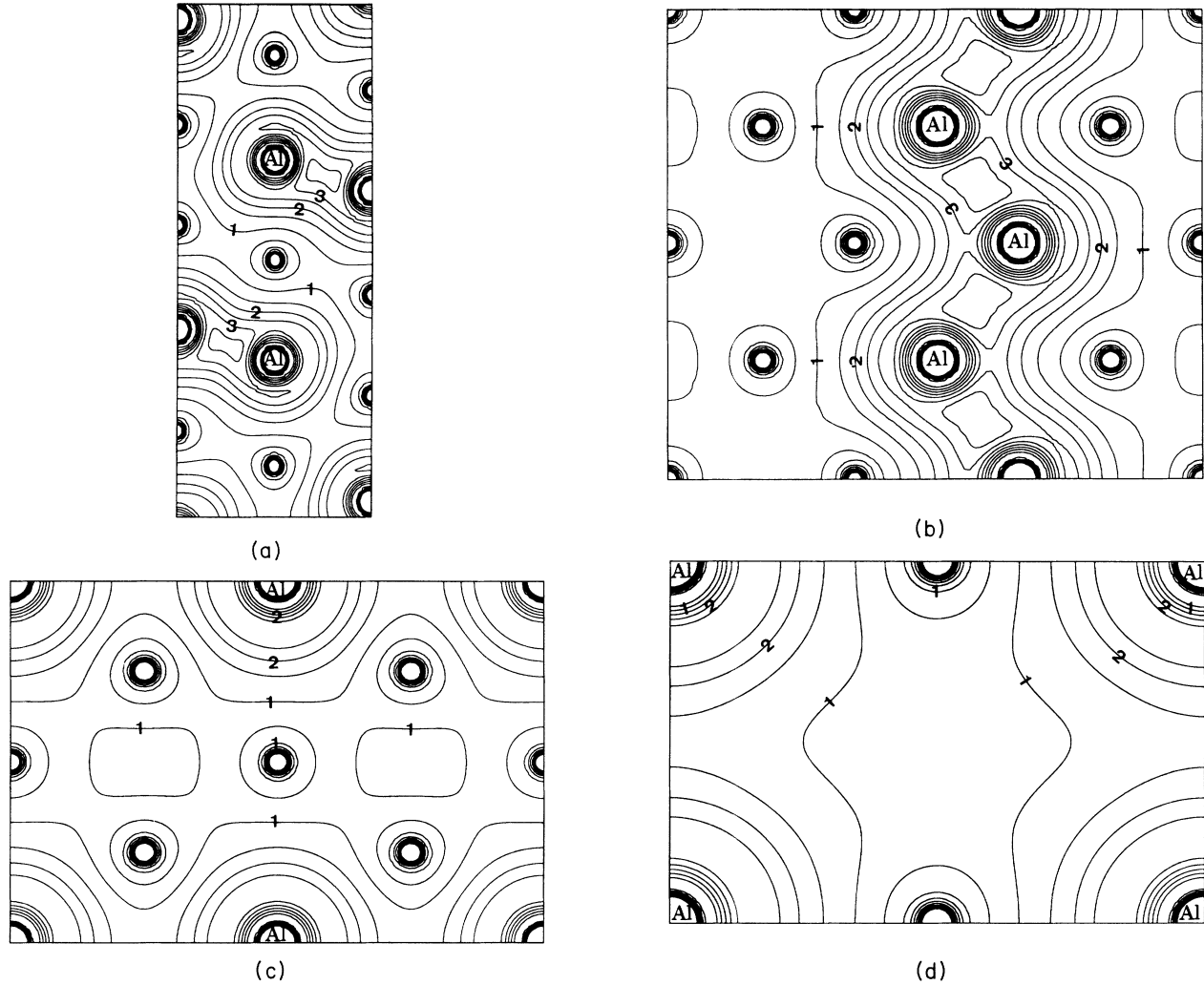


FIG. 3. Charge density contour plot in units of 10^{-2} (electrons)/(a.u.)³ for (a) Al_2Li_3 , (b) Al_4Li_9 , (c) AlLi_3 (D0_3) in the (110) plane, and (d) AlLi_3 (L1_2) in the (110) plane. Li atoms are characterized by their smaller size as compared to the larger-size Al atoms. In (a) the plane of contours is defined by the y - z plane, which cuts through the Al atoms perpendicular to the plane of drawings in Fig. 1(a). For (b) the plane of contours is defined by the atoms marked by c in Fig. 1(b).

TABLE VIII. Atomic distances (in a.u.) and the coordination number (CN) in Al_4Li_9 . Only neighbors of the Al atoms and Li (type 1) atom are shown.

Atom	Neighbor	Distance	CN	Atom	Neighbor	Distance	CN
Al(1)	Al(2)	4.952	2	Al(2)	Al(1)	4.952	2
	Li(1)	5.104	1		Li(1)	5.902	2
	Li(2)	5.555	1		Li(2)	5.018	2
	Li(2)	5.318	1		Li(3)	5.185	1
	Li(3)	5.242	1		Li(3)	6.066	2
	Li(3)	6.173	1		Li(4)	5.442	1
	Li(3)	5.939	2		Li(4)	5.807	1
	Li(4)	5.402	1		Li(5)	5.965	1
	Li(4)	5.159	2		Li(5)	5.145	1
	Li(4)	5.867	2		Li(5)	5.437	1
Li(1)	Al(1)	5.104	2				
	Al(2)	5.902	4				
	Li(2)	5.251	2				
	Al(2)	6.307	2				
	Li(5)	6.233	4				

nearest neighbor distance is 0.864, which is close to 0.866 for bcc. However, the nearest-neighbor distances vary greatly and some of the nearest neighbors are even close to the next nearest neighbors, which reflects the complexity of the Al_4Li_9 structure. The arrangement of Al atoms in this compound is peculiar. They form planar zigzag chains with the mean direction of all chains being parallel to the c axis. The Al-Al distances (4.952 a.u.) are the smallest nearest neighbor distances in the Al_4Li_9 compound, which is again much smaller than those in pure Al (7% smaller) and also smaller than those for B32-structure AlLi (3% smaller). The charge density contours [Fig. 3(b)] in the plane containing Al zigzag chains show a significant pileup of the charge between Al bonds, which is similar to the cases of Al_2Li_3 and B32-structure AlLi . This strong Al bond is again characteristic of the stable Al-Li ordered compounds.

On the other hand, there is no such pronounced Al—Al bonding effect in the AlLi_3 compounds, as shown in Figs. 3(c) and 3(d) (either for the Li_2 or DO_3 structure) since Al atoms are well separated by Li. The charge-density contours also show the more homogeneous distribution of the charge in these compounds. These structures are, therefore, unfavorable in forming the stable phases in the Li-rich side of the Al-Li alloys.

Based on a study of the AlLi and Al_3Li compounds,^{10,21} we proposed a simple model to describe the phase stability in the Al-Li system, i.e., that Li basically transfers its valence electron in between the Al bonds and the resultant strengthened Al bonds stabilize the Al-Li compounds. More specifically, the valence charge is redistributed (particularly in the interstitial region) to cause more of a pileup in Al bonds due to the Al-Al and Al-Li interactions. This simple model is further supported by the charge contour plots (Fig. 3) for Li-rich compounds. Under this assumption, we can derive two features for stable compounds on the Li-rich side. First, Al atoms tend to have Al nearest neighbors and form stronger bonds, even if the Li content is much larger than Al. This tendency might explain why Al-Li alloys do not stabilize in AlLi_3 compounds which have smaller unit cells and simpler crystal structures, but instead form more complicated Al_4Li_9 compounds.

Second, Al atoms tend to form tetrahedral diamondlike bonds due to the donation of electrons by Li, as in the perfect case of B32-structure AlLi . To see this tendency, let us compare the Al bonding characteristics in the B32-structure AlLi , Al_2Li_3 and Al_4Li_9 systems. As mentioned before, the Al_2Li_3 and Al_4Li_9 compounds, although quite complicated, can be viewed basically as having a distorted bcc structure. Figure 4 gives the Al position in a bcc (or distorted bcc) cube with one Al sitting in the center. For B32-structure AlLi , four Al nearest neighbor are located at the four opposite corners forming a perfect diamondlike bond. For Al_2Li_3 , three Al nearest neighbors are located at three of the four opposite corners, forming a three pronged diamondlike bond due to the deficit of Al atoms. For Al_4Li_9 , the Al atoms still tend to form diamondlike bonds, but the lack of Al atoms prevents them. As a result, two Al bonds are the best situation that can be formed for this compound. For Al_3Li compounds,

there is another supercell structure (eight atoms per cell), which was studied previously for the phase diagram calculation.⁵ Each Al atom also has two Al nearest neighbors in this 2:6 supercell structure. However, Al-Al atoms form a chain in the structure. Consequently, this structure is more stable than Li_2 and DO_3 , but is unstable relative to Al_4Li_9 .

IV. PHASE STABILITIES

Although the detailed electronic structure study can explain the physical origin of the phase equilibrium, it cannot directly determine the stable phases of the system in most situations. The thermodynamic functions are the fundamental quantities which govern the phase equilibria of the phase diagram.²² It is the free energy of formation that can determine the phase stability of the alloys. Phase equilibria in alloys is a more complex problem which is inherently nonlocal; the structure at fixed composition has to compete with the mixture of the neighboring compounds. Therefore the phase equilibrium should be determined by drawing common tangent²³ lines between the free energy curves of neighboring compounds.

The phase equilibrium at zero temperature on the Li-rich side of Al-Li alloys can be derived from the calculated total energy. At zero temperature, there is no entropy contribution to the free energy; therefore the free energy of formation, or heat of formation, is the difference in total energies between the compound and its constituent solids. The heat of formation of the compound A_xB_{1-x} is then defined as

$$\Delta H = E_{A_xB_{1-x}} - xE_A - (1-x)E_B, \quad (1)$$

where x is the composition, E_A and E_B are the total energies of the stable structures of pure A and B solids, and $E_{A_xB_{1-x}}$ is the total energy of the compound.

For pure Li, the situation is complicated. The stable structure of Li is bcc at temperatures above 77° K. Earlier work by Barrett *et al.*²⁴ suggested that Li undergoes a martensitic transformation to the hcp structure and probably to the fcc structure by cold working at low temperature.²⁵ However, a later study²⁶ showed that the ground-state structure is neither hcp nor fcc, but a 9R-related complex closepacked structure suggested by Overhauser.²⁷ Our calculations showed that fcc Li is more stable than bcc Li at zero temperature, but with only a very small energy difference (0.5 mRy). This indicates that the allotropic transformation in Li is possible at certain temperatures when the vibrational contribution plays a role, which is consistent with the experimental findings.

The heats of formation for all the Al-Li ordered compounds on the Li-rich side are shown in Fig. 5. Common tangent lines between stable compounds are also drawn in the figure. At $T=0$ K, the common tangent lines are those that connect the formation energies of two neighboring compounds with the assumption of stoichiometry. This figure explains very clearly the phase equilibria in the Al-Li system. One of the striking features is that it correctly predicts all the stable phases on the Li-rich side;

no other first-principles electronic-structure studies have ever made the correct prediction in this region. As shown in Fig. 5, the heat of formation for $B32$ -structure AlLi has the lowest value and hence $B32$ is the most stable phase in the Al-Li system. Actually this phase stays stable up to its melting point before disorder takes place.

The heat of formation for Al_2Li_3 lies below the common tangent line between $B32$ -structure AlLi and Al_4Li_9 ,

and therefore Al_2Li_3 is stable with respect to the mixture of $B32$ -structure AlLi and Al_4Li_9 . Furthermore, since these three ordered compounds can be considered as stoichiometric, the relative entropy change is small. Therefore the Al_2Li_3 phase can remain the stable phase up to relatively high temperatures (up to 793 K) in the experimental phase diagram.²⁸

The heat of formation for Al_4Li_9 lies below the common tangent line between Al_2Li_3 and pure Li. Hence

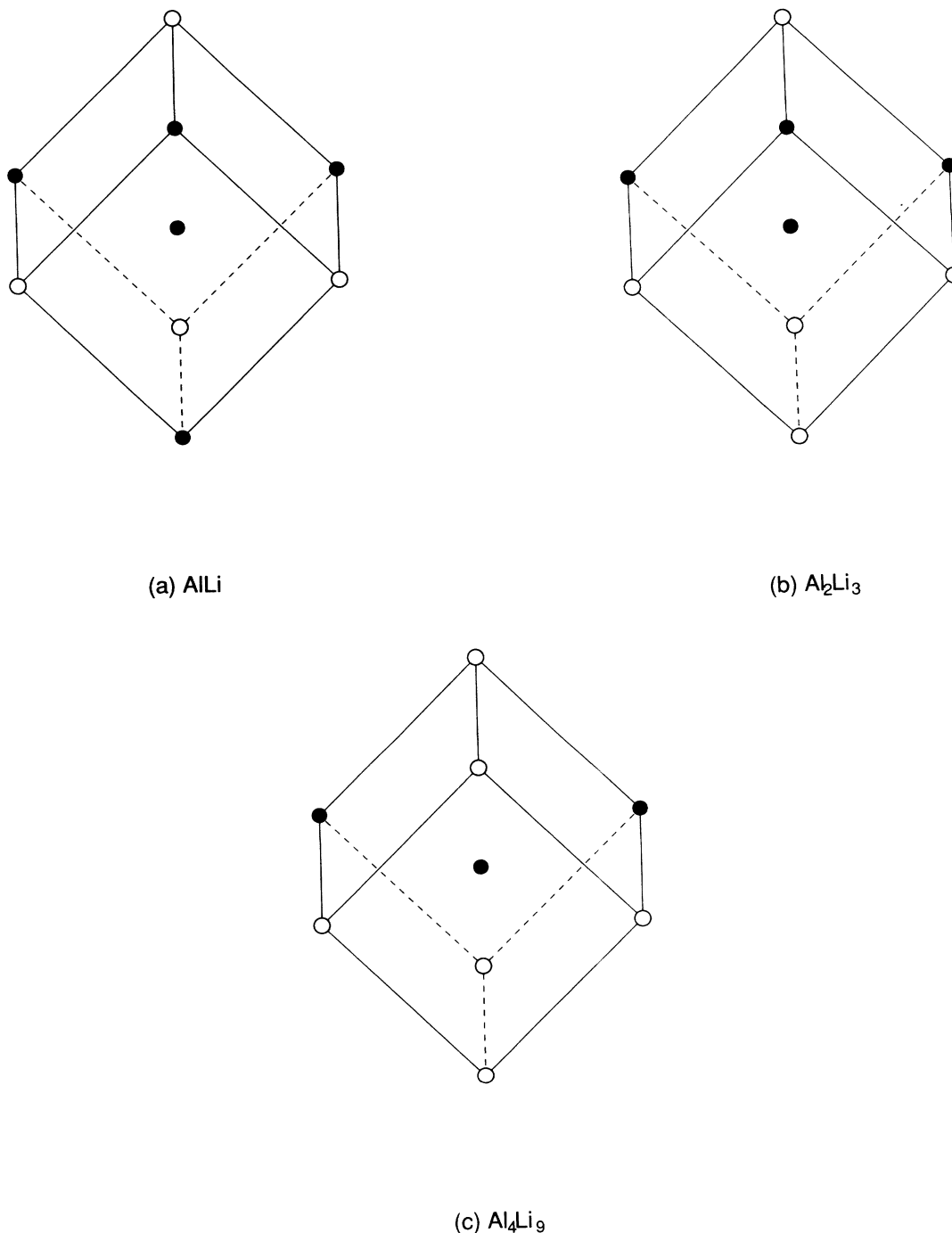


FIG. 4. Illustrative Al local environment in a bcc cube for (a) $B32$ -structure AlLi , (b) Al_2Li_3 , and (c) Al_4Li_9 .

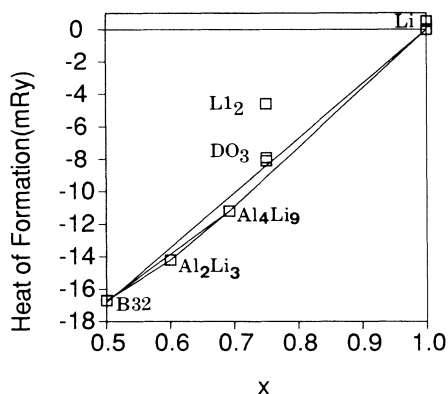


FIG. 5. Illustrative diagram of the heats of formation and the phase stability of Al-Li ordered compounds (at zero temperature).

Al_4Li_9 is stable with respect to the mixture of Al_2Li_3 and pure Li. However, when the temperature increases, the free energy of the AlLi solid solution (or even the AlLi liquid phase on the Li-rich side) decreases rapidly due to the pronounced contribution of the configurational entropy. Therefore the Al_4Li_9 phase can stay stable only at relatively low temperatures [603 K (Ref. 28)]. On the other hand, even though for the AlLi₃ compounds the DO_3 structure is more stable than the $L1_2$ structure, it is not a real stable phase in the Al-Li phase diagram; since its heat of formation is about 1.2 mRy per atom higher than that of the mixture of Al_4Li_9 and pure Li at the same average composition, it will decompose into those two phases in any case. Indeed, the DO_3 phase is never found to exist experimentally. Another fcc 2:6 supercell structure, although a bit more stable than DO_3 , is still an unstable structure with respect to the mixture of the neighboring compounds. All of the above findings corroborate the experimental results and demonstrate the re-

markable ability of highly precise band calculations to study the phase equilibria of the alloys (Table IX).

The phase diagram calculated by Sluiter *et al.*⁶ showed that DO_3 -structure AlLi₃ is a stable phase over some narrow range on the Li-rich side at the composition where Al_4Li_9 is located. However, this result only illustrates the fcc-bcc competition in Al-Li alloys and uses DO_3 as a representative for those complicated “interlopers” in which their structures were shown previously to be related to the bcc superstructure. To obtain more accurate, quantitative results, these two structures, Al_2Li_3 and Al_4Li_9 , should be included in the calculation of the phase diagram.

Since the calculation of phase diagrams is based on electronic band-structure total-energy calculations, the correct prediction of the stability sequence of these building blocks becomes most fundamental to the study. The correct phase diagram cannot be produced with any highly sophisticated statistical method if the stability sequence of these building blocks is wrong.

Finally, we need to emphasize that the Al-Li system is of theoretical importance since it can serve as a severe test for any method. Since both Al and Li are close-packed, free-electron-like simple metals, it is natural to expect that less precise methods such as the ASW, linear muffin-tin orbitals (LMTO), or pseudopotential methods should work well for this system. This might, however, not be the case. Indeed, the AlLi ordered compounds (i.e., 1:1 compounds) have been studied by a variety of methods over the years: for example, Christensen by LMTO,⁸ and Hafner and Weber by the linear confirmation of atomic orbitals (LCAO) method.⁹ These methods generally yield similar good results for the lattice constants and band structures except for some minor differences. The correct stability between the $B32$ and $B2$ structures is also produced because of the high stability of the $B32$ phase, although the quantitative energy difference varies significantly. However, when one stud-

TABLE IX. Equilibrium Wigner-Seitz radius (in a.u.), total energy (in Ry/atom) and bulk modulus (in Mbar) of some fcc and bcc superstructures of Al-Li compounds. Asterisks denote the stable phase at that composition. The dagger denotes the stability of Li is more complicated and has been discussed in the text.

Composition	Structure	Structure type	R_{WS}	E_{tot}	B_{calc}
Al	fcc*	fcc	2.9456	-483.8420	0.82
	bcc	bcc	2.9511	-483.8372	0.84
Al_3Li	$L1_2$ *	fcc	2.9357	-366.5986	0.72
	DO_3	bcc	2.9557	-366.5887	0.56
AlLi	$B32$ *	bcc	2.9104	-249.355	0.58
	$B2$	bcc	2.8760	-249.3488	0.42
	$L1_0$	fcc	2.9173	-249.3486	0.50
AlLi ₃	DO_3 *	bcc	2.9588	-132.0948	0.30
	$L1_2$	fcc	2.9647	-132.0915	0.28
Li	fcc*†	fcc	3.1246	-14.8352	0.14
	bcc	bcc	3.1276	-14.8347	0.15

ies the more sensitive properties such as formation energy, bulk modulus, and elastic constants, which involve much smaller energy differences, a more precise method is certainly needed for the Al-Li system; otherwise, incorrect results might be obtained.

Recently, Lu and Carlson²⁹ calculated the total energies of some Al-Li compounds by a simplified pseudopotential expansion theory. While pseudopotential theory has been successful in dealing with nearly-free-electron systems, it is difficult to apply to the Al-Li system because of the large density difference in Al and Li and the importance of the nonlocality of the pseudopotentials. In Lu and Carlson's calculation, the local-density correction to the usual second-order perturbation expansion and the treatment of the nonlocality of the pseudopotential are included to overcome these difficulties. As a result, they got fairly good results for some properties of the Al-Li compounds. For example, the calculated lattice constants are in good agreement with experiment; the lattice contraction of Al₃Li (*L*₁) and AlLi (*B*32) are found to

agree with experiment and with other theoretical calculations. The stability between the *B*32 and *B*2 structures also agrees with experiment. When studying the phase equilibria in the entire Al-Li system, they fail, however, to describe the correct phase diagram. According to their calculated heats of formation of some ordered Al-Li compounds, they predicted a much stabler Al₃Li (*L*₁) phase, an unstable Al₄Li₉ phase, and a metastable AlLi₃ *L*₁ phase (more stable than Al₄Li₉). All these predictions are inconsistent with the experiment, and with our results.

ACKNOWLEDGMENTS

This work was supported by the Air Force Office of Scientific Research (Grant No. 88-0346), U.S. Department of Defense, and by the Austrian Ministry of Science (Project No. 49-55313-24187). We are grateful to Dr. Marcel Sluiter for helpful discussions and collaboration on Ref. 6.

*Present address: Institute of Physical Chemistry, University of Vienna, Währingerstrasse 42, A-1090 Vienna, Austria.

¹Aluminum-Lithium Alloys, edited by T. H. Sanders, Jr. and E. A. Starke, Jr. (The Metallurgical Society of AIME, New York, 1981).

²Aluminum-Lithium Alloys II, edited by T. H. Sanders, Jr. and E. A. Starke, Jr. (The Metallurgical Society of AIME, New York, 1984).

³Aluminum-Lithium Alloys III, edited by C. Baker, P. J. Gregson, S. J. Harris, and C. J. Peel (The Institute of Metals, London, 1986).

⁴Aluminum-Lithium Alloys—Design, Development and Application Update, edited by R. J. Kar, S. P. Agrawal, and William E. Quist (ASM International, Metals Park, 1988).

⁵R. Podlucky, H. J. F. Jansen, X. Q. Guo, and A. J. Freeman, Phys. Rev. B **37**, 5478 (1988).

⁶M. Sluiter, D. de Fontaine, X. Q. Guo, R. Podlucky, and A. J. Freeman, in *Materials Research Society Symposia*, 1988 (MRS, Pittsburgh, in press); Phys. Rev. B **42**, 10460 (1990).

⁷E. Zintl and P. Wolterdorf, Z. Elektrochem, **41**, 876 (1935); E. Zintl and Brauer, Z. Phys. Chem. **20**, 245 (1935); W. Hüchel, *Structural Chemistry of Inorganic Compounds* (Elsevier, Amsterdam, 1951).

⁸N. E. Christensen, Phys. Rev. B **32**, 207 (1985).

⁹J. Hafner and W. Weber, Phys. Rev. B **33**, 747 (1986).

¹⁰X. Q. Guo, R. Podlucky, and A. J. Freeman, Phys. Rev. B **40**, 2793 (1989).

¹¹H. J. F. Jansen and A. J. Freeman, Phys. Rev. B **30**, 561 (1984).

¹²P. Hohenberg and W. Kohn, Phys. Rev. **136**, B864 (1964).

¹³W. Kohn and L. J. Sham, Phys. Rev. **140**, A1133 (1965).

¹⁴L. Hedin and B. I. Lundqvist, J. Phys. C **4**, 2064 (1971).

¹⁵K. Tebbe, H. G. V. Schnering, B. Rüter, and G. Rabeneck, Z. Naturforsch. B **28**, 600 (1973).

¹⁶T. Hong (private communication).

¹⁷Jianhua Xu (private communication).

¹⁸D. A. Hansen and J. F. Smith, Acta Crystallogr. Sect. B **24**, 913 (1968).

¹⁹American Institute of Physics Handbook, 2nd ed., edited by D. E. Gray (McGraw-Hill, New York, 1963).

²⁰V. L. Moruzzi, J. F. Janak, and K. Schwarz, Phys. Rev. B **37**, 790 (1988).

²¹X.-Q. Guo, R. Podlucky, Jian-hua Xu, and A. J. Freeman, Phys. Rev. B **41**, 12432 (1990).

²²W. Pitsch, in *Phase Stability in High Temperature Alloys*, edited by V. Guttman (Applied Science Publishers, London, 1981), p. 1.

²³For example, see *Physical Metallurgy*, 3rd ed., edited by R. W. Cahn and P. Haasen (North-Holland, Amsterdam, 1983).

²⁴C. S. Barrett and O. R. Trautz, Trans. Inst. Min. Metall. pet. Eng. **175**, 579 (1948).

²⁵C. S. Barrett, Phys. Rev. **72**, 245 (1947).

²⁶C. M. McCarthy, C. W. Thompson, and S. A. Werner, Phys. Rev. B **22**, 574 (1980).

²⁷A. W. Overhauser, Phys. Rev. Lett. **53**, 64 (1984).

²⁸A. J. McAlister, Bull. Alloy Phase Diagrams **3**, 177 (1982).

²⁹D. Lu and A. E. Carlson, Phys. Rev. B **40**, 980 (1989).